

# 基于归一化图像奇异值分解的焊接目标自动识别

李鹤喜<sup>1,2</sup>, 王国荣<sup>1</sup>, 石永华<sup>1</sup>, 张为民<sup>1</sup>

(1. 华南理工大学 机械工程学院, 广州 510640; 2. 五邑大学 信息工程学院, 广东 江门 529020)

**摘 要:** 提出了一种归一化图像矩阵奇异值分解来实现焊接目标的自动识别。为消除奇异值对图像方位和比例的依赖, 首先采用图像的二阶矩确定出焊接目标的主轴方向和长度, 然后将目标图像坐标旋转到主轴方向, 并按主轴长度进行尺寸归一化处理后再进行奇异值分解, 这样获得的图像奇异值将保持不变, 可以用作焊接目标识别的特征匹配。采用传统的直接奇异值分解和归一化奇异值分解对不同角度不同比例的平板焊件图像进行了对比识别试验, 同时还研究了图像灰度改变对奇异值的影响。结果表明, 归一化奇异值分解对目标图像的平移、旋转、比例和灰度变化表现了良好的稳定性, 能够用于焊接目标的自动识别。

**关键词:** 奇异值分解; 矩; 主轴; 焊接目标; 识别

**中图分类号:** TG409 **文献标识码:** A **文章编号:** 0253-360X(2008)02-0035-05



李鹤喜

## 0 序 言

近年来, 随着计算机技术、机器人技术和视觉传感器技术的相互融合, 大大加快了焊接技术的智能化, 在计算机控制下由焊接机器人自动完成整个焊接任务已成为智能焊接的发展趋势。实现智能化焊接的第一步是如何将焊矩自动地导入焊接目标区, 所以自动识别焊接目标就变得至关重要。目前焊接目标的识别基本上是依靠导航视觉传感器采集的图像信息和已建立起来的焊接目标图像比较来完成的。在机器视觉中, 刚体目标识别的常用方法是模板匹配和特征匹配。采用模板匹配, 计算量大, 同时由于目标对象在图像中方位不同, 模板必须平移和旋转。采用特征匹配, 必须找到有效的特征提取方法, Hu 矩作为刚体目标的几何特征是建立在二值图像的基础上, 可以作为焊接目标的特征提取<sup>[1]</sup>, 但 Hu 矩计算量大, 并且目标图像的二值化会丧失许多目标的细节信息, 此外环境光照不均匀, 会使同一目标二值化后的图像差异较大, 因此, 近年来, 很多图像识别与跟踪系统采用图像的奇异值分解(SVD)作为特征提取方法<sup>[2,3]</sup>, 这主要原因是图像矩阵的奇异值对图像灰度的波动表现了较强的鲁棒性, 同时图像的奇异值具有平移、转置和镜像不变性, 因此在

人脸识别、刚体目标跟踪系统中得到了广泛应用<sup>[4,5]</sup>。然而, 图像的奇异值分解对任意角度的目标旋转(非 90°的倍数)却不具有稳定性, 特别是长宽比相差较大的细长目标的图像奇异值在不同角度下差别很大, 这给摄像机从不同角度获得的目标的识别带来难度。为保持奇异值的旋转不变, 文献[6]提出从图像质心出发的射线方向来重构图像矩阵, 文献[7]采用极坐标进行旋转重构, 这两种方法都是对摄取的图像进行重构, 在多数情况下耗时很多, 为此提出了一种归一化的图像奇异值分解方法, 用于焊接目标的自动识别。其主要思想是利用图像的二阶矩确定焊接目标图像的主轴, 然后将图像坐标旋转与主轴重合, 再进行目标图像的奇异值分解, 为适应不同尺度的焊接目标图像, 以二阶矩决定的图像椭圆的长短轴来归一化图像尺寸(非外接椭圆), 这样获得的奇异值对不同角度获取的不同尺度的目标图像, 具有很高的稳定性, 以这样归一化的奇异值作为焊接目标的特征, 按相似判别准则就可以完成焊接目标的自动识别。

## 1 图像矩阵的奇异值分解原理

设像素尺寸为  $m \times n$  的图像灰度矩阵  $A \in R^{m \times n}$  ( $R$  为实数集), 则存在列向量正交的矩阵  $U = [u_1, u_2, \dots, u_m] \in R^{m \times m}$  和  $V = [v_1, v_2, \dots, v_n] \in R^{n \times n}$ , 即  $U^T U = I$ ,  $V^T V = I$  ( $I$  为单位矩阵), 使得

$$S = U^T A V = \begin{bmatrix} \Sigma & 0 \\ 0 & 0 \end{bmatrix} \quad (1)$$

式中: 对角矩阵  $\Sigma = \text{diag}(\sigma_1, \sigma_2, \dots, \sigma_p)$  的对角元素  $\sigma_i (i = 1, 2, \dots, p)$  称为  $A$  的奇异值 ( $p \leq \min\{m, n\}$ ), 而  $\sigma_i^2$  是矩阵  $AA^T$  的特征值,  $S$  称图像矩阵  $A$  的奇异值分解 (SVD, singular value decomposition)。在奇异值大于 0 的前提下, 奇异对角矩阵  $\Sigma$  的分解是唯一的。

奇异值分解具有下列特点: (1) 稳定, 对于矩阵  $A$  的数据元素微小的摄动, 其值变化小; 对图像而言, 对于灰度在一定的变化范围内具有鲁棒性。(2) 转置与镜像不变, 即图像旋转  $90^\circ, 180^\circ, 270^\circ$ , 奇异值不变。(3) 位移不变, 当目标图像在水平与垂直方向上任意平移, 奇异值不变。正是由于具有这些优点, SVD 作为图像的代数特征在刚体目标的跟踪与识别中得到了广泛应用。但主要存在的问题是 SVD 值对任意角度 (非  $90^\circ$  的倍数) 的旋转和比例缩放是变化的, 特别是对于长宽比大的目标图像, 旋转之后奇异值变化更为剧烈, 显然, 用奇异值作为图像的代数特征, 必须解决旋转和比例不变性。

## 2 焊接目标的主轴计算

在图像的几何形状特征分析中采用了在概率理论中使用的函数矩<sup>[8]</sup> (moments)。设像素为  $m \times n$  的数字图像在坐标  $(x, y)$  的灰度为  $A(x, y)$ , 则  $p+q$  阶矩可以表示为

$$M_{pq} = \sum_{x=1}^m \sum_{y=1}^n x^p y^q A(x, y) \quad (2)$$

为消除  $A(x, y)$  细节灰度之间的差别, 可以对图像进行均衡处理, 优化阈值, 然后转化为二值图像, 它反映了图像整体的几何特征。图像的中心坐标  $(x_c, y_c)$  可以表达为

$$x_c = \frac{M_{10}}{M_{00}}, \quad y_c = \frac{M_{01}}{M_{00}} \quad (3)$$

式中: 零阶矩  $M_{00}$  为所有像素之和;  $M_{10}, M_{01}$  为相对于  $x$  轴和  $y$  轴的一阶矩。图像相对于中心  $(x_c, y_c)$  的  $p+q$  阶中心矩为

$$\mu_{pq} = \sum_{x=1}^m \sum_{y=1}^n (x - x_c)^p (y - y_c)^q A(x, y) \quad (4)$$

图像的主轴方向一般规定为最小二阶中心矩的方向, 这里以试验中采用的平板焊接目标为例, 如图 1 所示,  $\theta$  为主轴与  $x$  轴的夹角,  $a, b$  为图像椭圆的长半轴与短半轴, 则有

$$\theta = \frac{1}{2} \arctan \left( \frac{2\mu_{11}}{\mu_{20} - \mu_{02}} \right) \quad (5)$$

式中:

$$\mu_{11} = \sum_{x=1}^m \sum_{y=1}^n (x - x_c)(y - y_c) A(x, y);$$

$$\mu_{20} = \sum_{x=1}^m \sum_{y=1}^n (x - x_c)^2 A(x, y);$$

$$\mu_{02} = \sum_{x=1}^m \sum_{y=1}^n (y - y_c)^2 A(x, y).$$

是相对中心  $(x_c, y_c)$  的二阶矩。

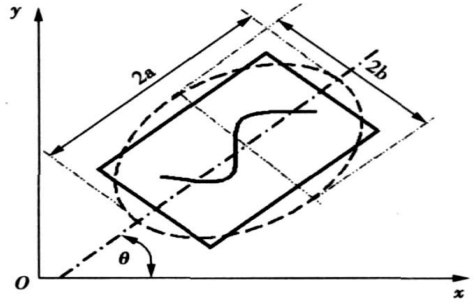


图 1 焊接目标的主轴

Fig. 1 Major axis of welding target

为适应不同尺度的焊接目标图像, 需要对图像尺寸进行归一化处理, 即进行比例缩放放到同一标准尺寸。可以用外接矩形或外接椭圆来做尺寸归一, 为使尺度归一具有统计意义上的稳定性, 这里采用的是二阶矩确定的图像椭圆的长短轴。图像椭圆长短半轴  $a, b$  由下式决定

$$\left. \begin{aligned} a &= \left\{ \frac{2[\mu_{20} + \mu_{02} + \sqrt{(\mu_{20} - \mu_{02})^2 + 4\mu_{11}^2}]}{M_{00}} \right\}^{\frac{1}{2}} \\ b &= \left\{ \frac{2[\mu_{20} - \mu_{02} + \sqrt{(\mu_{20} - \mu_{02})^2 + 4\mu_{11}^2}]}{M_{00}} \right\}^{\frac{1}{2}} \end{aligned} \right\} \quad (6)$$

## 3 焊接目标图像的归一化奇异值分解

在目标图像的识别与分类过程中, 都要建立标准的模板, 抽取模板的特征, 作为比较分类的基础。这里设焊接模板图像为  $A_0(x, y)$ , 并取模板惯性主轴夹角  $\theta_0 = 0$ , 按公式 (6) 计算出标准模板椭圆的长短轴  $a_0$  和  $b_0$ 。设待识别的焊接目标图像为  $A(x, y)$ , 则目标图像的归一化奇异值分解步骤如下: ① 将图像  $A(x, y)$  二值化处理, 按公式 (2) 计算图像的中心  $(x_c, y_c)$ ; ② 计算相对中心的二阶中心矩  $\mu_{11}, \mu_{20}, \mu_{02}$ ; ③ 按公式 (4) 和 (6) 计算主轴与  $x$  轴的夹角  $\theta$  以及椭圆的长短半轴  $a$  和  $b$ ; ④ 将图像坐标旋转到主轴方向, 即按逆时针方向旋转  $\theta$ ; ⑤ 计算目标

图像椭圆长短轴与模板长短轴的缩放比, 长轴缩放比  $R_l = a/a_0$ , 短轴缩放比  $R_s = b/b_0$ ; ⑥ 按长短轴缩放比, 将目标图像进行尺寸的归一化处理; ⑦ 按公式(1)进行目标图像的奇异值分解得到归一化的图像矩阵的奇异值  $\sigma_i (i = 1, 2, \dots, p)$ 。

通过这种归一化处理后, 目标图像的 SVD 对旋转、平移, 比例都会保持不变。需要指出的是, 在求主轴夹角和椭圆长短半轴时, 采用的是二值图像, 这是因为由于光照强度的差别即使是同质的目标图像的灰度也会有差别, 而在计算主轴时考虑的是图像区域面积的几何特征, 所以宜采用二值化处理消除灰度差别, 而 SVD 计算应采用灰度图像, 这样反映的是目标图像细节的本质特征。

4 奇异值相似判别准则

使用归一化奇异值分解完成焊接目标图像的特征提取, 对目标的识别就是和标准模板比较, 进行相似判别。常用的方法有欧氏距离相似度量准则和角度相似度量准则。欧式距离相似度量对奇异值向量的每个分量同等对待, 然而大家知道奇异值分量是按降序排列的, 小序号分量对目标特征起主导作用, 因此这里提出一种加权相似度  $J$  作为奇异值相似的判别准则。设焊接目标模板的归一化奇异值分解向量为  $S_0 = \{\sigma_{01}, \sigma_{02}, \dots, \sigma_{0n}\}$ , 待识别的焊接目标的奇异值向量为  $S = \{\sigma_1, \sigma_2, \dots, \sigma_n\}$ , 则两向量的相似度  $J$  由下式决定

$$J = \frac{\sum_{i=1}^n [1 - \frac{\sigma_i - \sigma_{0i}}{\max(\sigma_i, \sigma_{0i})}] w(i)}{\sum_{i=1}^n w(i)} \tag{7}$$

式中:  $n$  为奇异值向量的长度, 由于奇异值的降序排列, 靠后的分量很小, 可以截取前  $N$  个分量;  $|\sigma_i - \sigma_{0i}|/\max(\sigma_i, \sigma_{0i})$  为每个分量的相对误差;  $1 - |\sigma_i - \sigma_{0i}|/\max(\sigma_i, \sigma_{0i})$  为相似系数;  $w(i)$  为加权系数, 这里取  $w(i) = 1 - (i/n)$  按降序排列。当待识别焊接目标与标准模板完全相同时  $J = 1$ , 所以  $J$  接近 1 的程度反映了待识别焊接目标与标准模板的相似程度, 一般根据匹配的精度选取一个  $J$  的合适阈值  $J_T$ , 当  $J > J_T$  时, 即检测到焊接目标。

5 试验结果与讨论

试验的主要目的有两个, 一是研究当焊接机器人以不同方向接近焊接对象, 即获取的图像角度变化和尺度变化时, 采用直接奇异值分解 DSVD(Direct






SVD)和提出的归一化奇异值分解 NSVD(Normalized SVD)与标准模板奇异值的偏差, 从而验证所建议识别方法的可行性; 二是改变环境照度, 使焊接目标图像的灰度在一定范围变化, 考察奇异值分解的鲁棒性及其对识别结果的影响。焊接目标为含有曲线焊缝矩形平板, 尺寸为 360 mm×120 mm, 视觉传感器为小型 320×240 的 CCD 摄像机, 安装在焊接机器人末端, 焊接背景固定, 采用二维多尺度分析进行目标图像的滤波预处理, 消除细节和孤立噪声。应用背景差分 and 轮廓检测相融合的方法从背景中提取焊接目标。

5.1 焊接目标旋转与尺度变化条件下 NSVD 和 DSVD 的比较

用“ $\theta/R =$  角度/缩放比”来表示焊接平板图像的旋转程度(方位)和比例大小,  $\theta$  为平板焊件主轴与  $x$  轴夹角,  $R = R_l = R_s$  (设长短轴缩放比相同)为相对模板的缩放比例。这里取标准模板的  $\theta/R = 0^\circ/1.0$ , 对  $\theta/R = 30^\circ/0.8$ ,  $\theta/R = 45^\circ/0.9$ ,  $\theta/R = 60^\circ/1.2$  和  $\theta/R = 90^\circ/1.3$  四种不同角度不同比例的焊接平板图像, 进行了 DSVD 直接奇异值分解和按图像主轴方向的 NSVD 归一化奇异值分解, 表 1 和表 2 给出了两种 SVD 结果的奇异值(SV)前 10 项。

表 1 不同  $\theta/R$  下的直接奇异值分解结果

Table 1 DSVD results at different  $\theta/R$  values





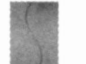
	模板 $0^\circ/1.0$	$30^\circ/0.8$	$45^\circ/0.9$	$60^\circ/1.2$	$90^\circ/1.3$
奇异值					
$\sigma_1$	98.722 3	82.795 2	80.062 0	82.761 9	98.723 0
$\sigma_2$	10.883 4	41.949 1	45.572 9	41.862 1	10.883 4
$\sigma_3$	6.082 9	19.130 2	18.816 9	19.323 6	6.082 5
$\sigma_4$	5.270 5	16.449 1	13.987 7	16.132 9	5.271 2
$\sigma_5$	4.246 8	10.804 4	13.572 8	11.197 6	4.246 7
$\sigma_6$	3.742 0	10.369 0	11.120 5	10.574 5	3.742 1
$\sigma_7$	3.593 9	7.863 4	9.449 9	7.648 4	3.594 1
$\sigma_8$	1.893 4	6.521 5	9.176 0	6.509 2	1.892 9
$\sigma_9$	1.782 7	6.080 6	7.354 0	6.112 5	1.782 7
$\sigma_{10}$	1.683 6	5.821 4	6.490 1	5.812 5	1.683 3

从表 1 和表 2 中的数据明显地看出, 当平板的旋转角度与图像尺度不同时直接分解的奇异值相差很大, 而按沿主轴归一化分解的奇异值变化很小。

两种奇异值分解与模板奇异值偏差变化曲线如图 2 所示, 纵轴为不同角度奇异值与模板奇异值的偏差  $E = |\sigma_i - \sigma_{i0}|$ , 横轴为奇异值分量的序号  $i$ 。

图 2 表明, 归一化奇异值分解最大偏差不超过 1.4, 并且出现在第 7 个奇异值分量, 而直接奇异值

表 2 不同  $\theta/R$  值下的归一化奇异值分解结果  
Table 2 NSVD results at different  $\theta/R$  values

	模板 $0^\circ/1.0$	$30^\circ/0.8$	$45^\circ/0.9$	$60^\circ/1.2$	$90^\circ/1.3$
奇异值					
$\sigma_1$	98.722 3	98.838 6	98.825 0	98.844 8	98.723 0
$\sigma_2$	10.883 4	10.503 0	10.547 4	10.416 1	10.883 4
$\sigma_3$	6.082 9	5.603 5	5.594 5	5.479 9	6.082 5
$\sigma_4$	5.270 5	4.690 3	4.639 1	4.594 0	5.271 2
$\sigma_5$	4.246 8	3.356 9	3.301 7	3.258 2	4.246 7
$\sigma_6$	3.742 0	2.777 9	2.883 0	2.772 6	3.742 1
$\sigma_7$	3.593 9	2.375 4	2.368 9	2.298 8	3.594 1
$\sigma_8$	1.893 4	1.838 0	1.841 9	1.838 3	1.892 9
$\sigma_9$	1.782 7	1.801 6	1.799 8	1.758 9	1.782 7
$\sigma_{10}$	1.683 6	1.699 0	1.678 4	1.661 1	1.683 3

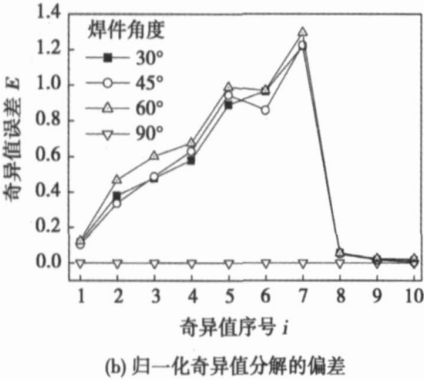
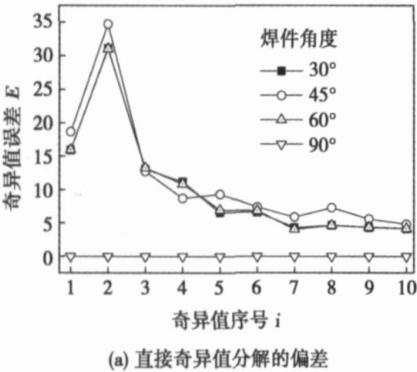


图 2 直接与归一化 SVD 的奇异值偏差

Fig.2 Singular value errors for DSVD and NSVD




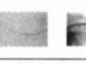

分解最大偏差达 35, 偏差超过 30%, 并且出现在第 2 个奇异值分量, 大家知道, 奇异值按降序排列, 小序号奇异值决定特征的主体, 偏差最大出现的序号越小, 与模板的相似性越小, 所以无论从最大偏差的绝对值, 还是出现序号大小, 都表明归一化奇异值分解与模板奇异值保持很好的一致性, 而直接奇异值分解在  $30^\circ, 45^\circ, 60^\circ$  产生的偏差太大并且都是在小序号产生的, 与模板没有相似性, 因此这样条件下直接 SVD 分解已失去意义, 无法用于焊接目标的识别。

当旋转角度为  $90^\circ$  时, 两者相同, 都与模板保持一致, 这是由 SVD 的转置不变性决定的。

5.2 灰度变化对奇异值的影响

在焊接平板方位不变的条件下, 人为改变环境的照度, 变化幅度从低到高依次获得 5 个灰度等级的焊接平板图像, 灰度均值依次是 182, 192, 201, 212 和 240, 它们的前 10 个奇异值如表 3 所示(模板奇异值和表 1 相同, 未列出)。图 3 是对应不同灰度的奇异值分量与模板奇异值偏差  $E$  的变化曲线。

表 3 不同灰度均值下的归一化奇异值分解结果  
Table 3 NSVD results at different gray levels

	灰度均值 (182)	灰度均值 (192)	灰度均值 (201)	灰度均值 (212)	灰度均值 (240)
奇异值					
$\sigma_1$	99.177 1	99.190 1	100.504 3	103.574 7	124.708 6
$\sigma_2$	10.898 1	10.932 7	11.084 3	11.650 2	13.757 5
$\sigma_3$	5.974 2	6.107 1	6.163 8	7.530 0	7.550 6
$\sigma_4$	4.933 2	5.289 5	5.263 1	6.353 1	6.313 5
$\sigma_5$	3.997 4	4.259 8	4.253 5	5.552 1	5.086 8
$\sigma_6$	3.731 0	3.755 1	3.764 3	4.656 4	4.640 0
$\sigma_7$	3.518 3	3.611 0	3.674 9	3.872 4	4.422 4
$\sigma_8$	1.873 1	1.899 1	1.927 1	2.808 7	2.381 6
$\sigma_9$	1.623 4	1.782 6	1.769 3	2.725 4	2.056 8
$\sigma_{10}$	1.397 4	1.686 9	1.692 8	2.567 2	1.989 6

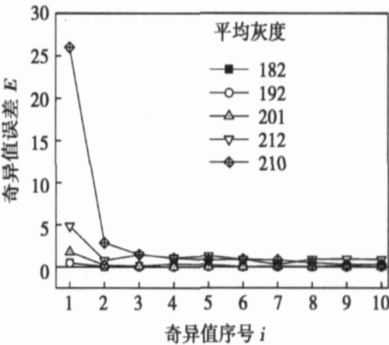


图 3 不同灰度下归一化 SVD 的奇异值偏差

Fig.3 Singular value errors under different gray levels

从图 3 可以看出, 当灰度在一定的范围波动(灰度均值为 182, 192, 201, 212), 产生的误差小于 5 (5%), 而当灰度变化特别剧烈(灰度均值 240), 误差为 26, 超过了 25%。与旋转变化的不同的是灰度的最大偏差出现在第一个分量上, 所以要给予特别重视。不过可以在图像处理上采取灰度均衡等方法降低它对 SVD 稳定性的影响。总体而言, 归一化奇异值分解对灰度波动呈现较好的鲁棒性。

5.3 识别结果

设奇异值相似准则的阈值  $J_T = 0.85$ , 根据表 1、表 2 和表 3 的奇异值分解数据, 按相似准则公式(7)计算的平板焊接目标的识别结果列于如表 4 和表 5, Y 表示可以识别, N 表示不可识别。

表 4 采用归一化奇异值分解的识别结果

Table 4 Recognition results using NSVD

$\theta/R$ 或平均灰度	相似度 $J$	识别结果(Y/N)
$30^\circ/0.8$	0.902 6	Y
$45^\circ/0.9$	0.907 6	Y
$60^\circ/1.2$	0.886 8	Y
$90^\circ/1.3$	0.999 7	Y
182(以下为灰度均值)	0.976 9	Y
192	0.996 1	Y
201	0.987 9	Y
212	0.855 8	Y
240	0.808 8	N

表 5 采用直接奇异值分解的识别结果

Table 5 Recognition results using DSVD

$\theta/R$	相似度 $J$	识别结果(Y/N)
$30^\circ/0.8$	0.365 2	N
$45^\circ/0.9$	0.344 8	N
$60^\circ/1.2$	0.376 1	N
$90^\circ/1.3$	0.999 8	Y

从表 4 的结果可以看出, 采用归一化奇异值分解, 可以对旋转、尺度变化和小范围灰度变化的焊接目标进行识别, 只有当灰度变化剧烈时, 奇异值改变较大, 这种方法失效。一般对于比较稳定的光照环境, 这种建议的方法还是十分有效的。表 5 的结果表明除旋转  $90^\circ$  的特例(转置不变), 当平板旋转  $30^\circ$ ,  $45^\circ$  和  $60^\circ$  都是不能识别的, 说明直接奇异值分解不能用于焊接目标的自动识别。

6 结 论

(1) 图像矩阵的奇异值分解, 随目标图像的方

位和比例的不同而改变, 不能直接用于焊接目标的自动识别。

(2) 将焊接目标图像旋转到主轴方向并根据图像椭圆长短轴尺寸进行图像尺度的归一化处理后, 再进行奇异值分解, 可以消除图像方位和比例变化的影响, 使获得的奇异值具有平移、旋转和比例不变性。

(3) 目标图像的灰度在一定范围变化, 归一化奇异值改变很小, 表现了很好的鲁棒性。

(4) 通过对平板焊接目标的识别试验, 验证了归一化奇异值分解方法作为目标图像特征提取的有效性, 可以用于智能化焊接系统中焊接目标的自动识别。

(5) 采用加权相似准则, 更好地反映了不同大小的奇异值对识别结果的影响。

参考文献:

[ 1 ] Hu M K. Visual pattern recognition by moment invariants[ J ]. IEEE Transactions on Information theory, 1962, 8: 179—187.

[ 2 ] Hong Z Q. Algebraic feature extraction of image for recognition[ J ]. Pattern Recognition, 1991, 24: 211—219.

[ 3 ] 于海征. 基于奇异值分解的数字图像特征提取[ J ]. 工程数学学报, 2004, 21(8): 131—134.

[ 4 ] 史泽林, 张志佳, 黄莎白. 基于奇异值分解的图像匹配及目标跟踪研究[ J ]. 小型微型计算机系统, 2005, 26(9): 1643—1646.

[ 5 ] 李竹林, 张根耀, 赵宗涛, 等. 奇异值特征在目标识别中的应用[ J ]. 微电子学与计算机, 2004, 21(11): 27—28.

[ 6 ] 邬永革, 丁 震, 黄 炯, 等. 一种有效的图像特征抽取和识别方法[ J ]. 计算机研究与发展, 1997, 34(1): 38—42.

[ 7 ] 石雅铮, 金声震, 宁书年, 等. 图像矩阵奇异值旋转不变性的重建[ J ]. 中国图像图形学报, 2005, 10(6): 717—720.

[ 8 ] Sonka M, Hlavac V, Boyle R. Image processing, analysis and machine vision(second edition)[ M ]. USA: Brooks/Cole, Thomson Ltd, 2001.

作者简介: 李鹤喜, 男, 1962 年出生, 博士研究生, 副教授。主要从事智能控制、模式识别方面的科研和教学工作。发表论文 9 篇。  
Email: lhx\_wq@sina.com

**Abstract** 2519 high strength aluminum alloy was welded with metal inert-gas welding process, and the effect of heat input on the microstructure, mechanical properties and fracture characters of the welds were studied. Results indicate that with the increase of the heat input, the second dendrite arm spacing increase and the content of solute in dendrite core decrease. After aging, the number of  $\theta'$  phase decrease, but its size increase. And the morphology of the eutectic phase changes from low rod type to long band network type with the increase of heat input, which causes the fracture type from transgranular to intergranular. The tensile strength reduces greatly with the increase of heat input, and the improvement of tensile strength is greater under low heat input condition after aging treatment.

**Key words:** high strength aluminum alloy; heat input; microstructure; fracture

### **Influence of diode-laser soldering procedure on mechanical properties and microstructure of Sn-Ag-Cu soldered joint**

ZHANG Xin, XUE Songbai, HAN Zongjie, HAN Xianpeng (College of Materials Science and Technology, Nanjing University of Aeronautics and Astronautics, Nanjing 210016, China), p22–26

**Abstract:** Using different diode-laser soldering parameters, soldering experiments of Sn-Ag-Cu lead-free solder was carried out on Cu substrate using diode-laser soldering system, and the forming rules of the intermetallic compound were also analyzed in Sn-Ag-Cu soldered joints. The results show that, when the laser soldering time is 1s and the laser output power is 38.3 W, the mechanical properties of soldered joints are the best. With the change of laser soldering parameters, microstructures of soldered joints are relevantly changed. With the optimum laser soldering parameters, microstructures of soldered joint are fine and no excessive grow of  $\text{Cu}_6\text{Sn}_5$  intermetallic compound, and the appropriate thickness of  $\text{Cu}_6\text{Sn}_5$  layer is also got. Competitive experiments results show the intermetallic compound layer with laser soldering system is smoother than that with the IR soldering method, and the excellent mechanical properties can be obtained for the soldered joints.

**Key words:** diode laser soldering; lead-free soldered joint; intermetallic compound; microstructure

### **3D heat transfer model in laser deep penetration welding based on real keyhole**

ZHANG Yi, CHEN Genyu, LI Lijun (State Key Laboratory of Advanced Design and Manufacturing for Vehicle Body, Hunan University, Changsha, 410082, China), p27–30

**Abstract** The heat transfer in laser deep penetration welding includes heat conduction and convection in the welding pool. A 3D heat transfer model in laser deep penetration welding was developed. The main characteristics of the model has some characteristics as follows: (1) A prototype of the keyhole in the model was obtained from the experiments. (2) The convection and the temperature distribution in the depth were considered. (3) The same law in the solid

and the liquid region, i. e. the viscosity of the material in the solid region was infinite; however the viscosity of the material in the liquid region was set to actual value. The model was solved by a finite element method, and the results show that: The isotherms in laser welding are shaped as ellipses. The temperature gradient and the velocity gradient on the front keyhole wall are greater than those on the rear keyhole wall. The convection flow in the welding pool is driven by the surface tension.

**Key words:** laser welding; heat transfer; mathematical model

### **Effect of heat treatment on microstructure and mechanical properties of high strength aluminum alloy welds**

XU Lianghong, TIAN Zhilings, PENG Yun, ZHANG Xiaomu (State Key Laboratory of Advanced Steel Processes and Products, Centre Iron & Steel Research Institute, Beijing 100081, China), p31–34

**Abstract** 2519 high strength aluminum alloy was welded, and the effect of aging treatment and solution treatment on the microstructure and mechanical properties were investigated. Results indicate that the aging treatment is helpful to improve the tensile strength of the joints, when the aging temperature is 150 °C, and the tensile strength of the joints reach its max value. The tensile strength of the joints can be improved greatly by solution treatment, and with the increase of the solution temperature, the tensile strength of the joints increases. However, when the temperature reaches 540 °C, liquid crack easily occurs, and the tensile strength will be decreased. The solution temperature can be improved to 540 °C by strength solution treatment, and the strength can reach 93% of that of the base metal.

**Key words:** high strength aluminum alloy; heat treatment; microstructure; aging

### **Automatic recognition of welding targets based on normalized singular value decomposition of image matrix**

LI Hexi<sup>1,2</sup>, WANG Guorong<sup>1</sup>, SHI Yonghua<sup>1</sup>, ZHANG Weimin<sup>1</sup> (1. College of Mechanical Engineering, South China University of Technology, Guangzhou 510640, China; 2. College of Information Engineering, Wuyi University, Jiangmen 529020, Guangdong, China), p35–39

**Abstract** A normalized singular value decomposition (SVD) of image matrix was presented for the automatic recognition of welding targets. In order to eliminate the dependence of SVD on the orientation and scale of a target image, the direction and length of the major axis of the target image were first determined using the 2nd-order moments, and the x-coordinate of the target image was rotated to the direction of major axis and the length of major axis was normalized, and then the SVD of the target image was completed, and the singular value obtained by the normalized SVD method can be used as the feature matching of welding target recognition because of its stability. The contrastive recognition experiments were made using the conventional direct SVD and proposed normalized SVD for a planar weldment image with different orientations and scales. In addi-

tion, the effect of the target image brightness on SVD was also investigated. The experimental results shown that the normalized SVD method has high stability to the translation, rotation, scale and brightness of target images and can be applied to the automatic recognition of welding targets.

**Key words:** singular value decomposition; moment; major axis; welding target; recognition

**Experimental modeling on steady-state vibration of bonding tool in ultrasonic bonding** CHENG Bao, HAN Lei (College of Mechanical and Electrical Engineering, Central South University, Changsha 410083, China). p40—44

**Abstract** The sinusoidally excited vibration of bonding tool at measurement for a ultrasonic load was measured by continuously scanning laser Doppler vibrometer PSV-400-M2 (1.5 MHz). The experimental phenomena and scanning testing results showed the steady-state vibration show uncertainty when the tightness changes; under the same tightness there is single-node in vibration, but under different tightness the node positions have changed; the velocity amplitude is not as the largest as expectation. In addition, the mathematics modeling was carried out based on the vibration theory of flexible beam.

**Key words:** ultrasonic bonding; tightness; laser doppler vibrometer; scanning

**Effect of gallium on microstructure and mechanical properties of Ag-Cu-Zn filler metals** HAN Xianpeng<sup>1,2</sup>, XUE Songbai<sup>1,2</sup>, GU Liyong<sup>3</sup>, GU Wenhua<sup>3</sup>, ZHANG Xin<sup>1</sup> (1. College of Materials Science and Technology, Nanjing University of Aeronautics and Astronautics, Nanjing 210016, China; 2. Province Key Laboratory of Advanced Welding Technology, Jiangsu University of Science and Technology, Zhenjiang 212003, Jiangsu, China; 3. Changshu Huayin Filler Metals Co., Ltd., Changshu 215513, Jiangsu, China). p45—48

**Abstract** Spreadability, microstructures and mechanical properties of brazed joints of silver filler metals with different content of gallium were studied. The results show that silver filler metals with excellent spreadability and sound mechanical properties of brazed joint can be developed by optimizing the compositions of silver filler metals with gallium. By using brass plates as base metal and brazing with flame method, the mechanical properties of the joints brazed with lap-joint and butt joint were examined and analyzed. The results indicate that the fractures of two kinds of brazed joints had happened on the base metal, which shows better mechanical properties of the joints brazed with the silver filler metals with gallium and an substituted the silver filler metals with cadmium completely.

**Key words:** silver filler metal; spreadability; mechanical property; microstructure

**Wettability and interfacial reaction product of electron beam**

**brazing of Ni-base superalloys K465** WANG Gang<sup>1</sup>, ZHANG Binggang<sup>1</sup>, FENG Jicai<sup>1</sup>, HE Jingshan<sup>1</sup>, MA Yibin<sup>2</sup> (State Key Laboratory of Advanced Welding Production Technology, Harbin Institute of Technology, Harbin, 150001, China; 2. Institute of Space Medicoengineering, Beijing 100094, China). p49—52, 56

**Abstract** The vacuum electron beam brazing (VEBB) of Ni-base superalloys with Bp27 and BNi-2 filler metals was studied. In process of VEBB, effects of primary brazing parameters on wettability and selection of filler metals were investigated, then it points out that electron beam current is the most significant factors. Moreover, microstructure of brazed joint with Bp27 filler metal was studied by means of scanning electron microscope, energy disperse spectrum and X-ray diffraction. The investigation shows that the structure of brazing seam consists of a large amount of  $\gamma$  solid solution, a large amount of  $\text{Ni}_3\text{B}$  and  $\text{CrB}$  rich in W, and a small quantity of  $\text{NbC}$ .

**Key words:** electron beam; brazing; wettability; interfacial reaction product

**Effect of magnetic field frequency on properties of Fe5 surfacing metal** LIU Zhengjun<sup>1</sup>, SU Yunhai<sup>1</sup>, LU Hailong<sup>2</sup> (1. School of Materials Science and Engineering, Shenyang University of Technology, Shenyang, 110023; 2. School of Jilin industry profession technique, Jilin, 132013). p53—56

**Abstract** The Fe5 alloy was overlaid on low carbon steel by plasma arc with longitudinal magnetic field. The scanning electron microscope, wear loss test, micro-hardness test were used to analyze the effect of magnetic field frequency on properties of surfacing metal. The results indicate that electromagnetic stirring can improve the shape and distribution of hard phase and refine the primary crystallization structure. The hardness and wear resistance vary with magnetic field frequency. The properties of surfacing metal are improved when the magnetic field frequency in an optimal value.

**Key words:** plasma arc surfacing; longitudinal magnetic field; electromagnetic stirring; magnetic frequency

**Influence of rare earths on Fe-based amorphous composite coatings by laser cladding** ZHU Qingjun, ZOU Zengda, WANG Xinhong, QU Shiyao (School of Materials Science and Engineering, Shandong University, Jinan 250061, China). p57—60

**Abstract** The influence of rare earths (RE) on the laser cladded Fe-based amorphous composite coatings was investigated by micro alloying. X-ray diffraction and scanning electron microscopy was used to study the phase, microstructure and the influence of RE on the fabrication of the amorphous phase. The results show that the glass formation ability of the  $\text{Fe}_{38}\text{Ni}_{30}\text{Si}_{16}\text{B}_{14}\text{V}_2$  amorphous alloy can be enhanced by micro alloying of RE which is helpful for the synthesis of the amorphous phase under the condition of laser cladding. The crystallization system of the amorphous alloy is changed by the addition of RE. It enhances crystallization of the  $\gamma$ -Fe, Ni phase and depresses the crystalline of  $\text{Fe}_2\text{B}$  phase while the